

---

# Input margins can predict generalization too

---

Coenraad Mouton<sup>1,2,3</sup> Marthinus W. Theunissen<sup>1,2</sup> Marelle H. Davel<sup>1,2,4</sup>  
<sup>1</sup>North-West University <sup>2</sup>CAIR <sup>3</sup>SANSA <sup>4</sup>NITheCS  
{moutoncoenraad, tiantheunissen, marelle.davel}@gmail.com

## Abstract

Understanding generalization in deep neural networks is an active area of research. A promising avenue of exploration has been that of margin measurements: the shortest distance to the decision boundary for a given sample or its representation internal to the network. While margins have been shown to be correlated with the generalization ability of a model when measured at its hidden representations (hidden margins), no such link between large margins and generalization has been established for *input margins*. We show that while input margins are not generally predictive of generalization, they can be if the search space is appropriately constrained. We develop such a measure based on input margins, which we refer to as ‘constrained margins’. The predictive power of this new measure is demonstrated on the ‘Predicting Generalization in Deep Learning’ (PGDL) dataset and contrasted with hidden representation margins. We find that constrained margins achieve highly competitive scores and outperform other margin measurements in general. This provides a novel insight on the relationship between generalization and classification margins, and highlights the importance of considering the data manifold for investigations of generalization in DNNs.

## 1 Introduction

Our understanding of the generalization ability of deep neural networks (DNNs) remains incomplete. Various bounds on the generalization error for classical machine learning models have been proposed based on the complexity of the hypothesis space [1, 2]. However, this approach paints an unfinished picture when considering modern DNNs [3]. Generalization in DNNs is an active field of study and updated bounds are proposed on an ongoing basis [4, 5, 6, 7].

A complementary approach to developing theoretical bounds is to develop empirical techniques that are able to predict the generalization ability of certain families of DNN models. The ‘Predicting Generalization in Deep Learning’ (PGDL) challenge, exemplifies such an approach. The challenge was held at NeurIPS 2020 [8] and provides a useful test bed for evaluating *complexity measures*, where a complexity measure is a scalar-valued function that relates a model’s training data and parameters to its expected performance on unseen data. Such a predictive complexity measure would not only be practically useful but could lead to new insights into how DNNs generalize.

In this work, we focus on classification margins in deep neural classifiers. It is important to note that the term ‘margin’ is, often confusingly, used to refer to 1) output margins [9], 2) input margins [10], and 3) hidden margins [11], interchangeably. Here (1) is a measure of the difference in class output values, while (2) or (3) is concerned with measuring the distance from a sample to its nearest decision boundary in either input or hidden representation space, respectively. In this work, we focus on input and hidden margins.

While margins measured at the hidden representations of deep neural classifiers have been shown to be predictive of a model’s generalization, this link has not been established for input space margins. We show that, in several circumstances, the classical definition of input margin does *not* predict

generalization, but a direction-constrained version of this metric does: a quantity we refer to as *constrained margins*. By measuring margins in directions of ‘high utility’, that is, directions that are expected to be more useful to the classification task, we are able to better capture the generalization ability of a trained DNN.

We make several contributions:

1. Demonstrate the first link between large input margins and generalisation performance, by developing a new input margin-based complexity measure that achieves highly competitive performance on the PGDL benchmark and outperforms several contemporary complexity measures.
2. Show that margins do not necessarily need to be measured at multiple hidden layers to be predictive of generalization, as suggested in [11].
3. Provide a new perspective on margin analysis and how it applies to DNNs, that of finding high utility directions along which to measure the distance to the boundary instead of focusing on finding the shortest distance.

## 2 Background

This section provides an overview of existing work on 1) measuring classification margins and their relationship to generalization, and 2) the PGDL challenge and related complexity measures.

### 2.1 Classification Margins and Generalization

Considerable prior work exists on understanding classification margins in machine learning models [12, 13]. The relation between margin and generalization is well understood for classifiers such as support vector machines (SVMs) under statistical learning theory [1]. However, the non-linearity and high dimensionality of DNN decision boundaries complicate such analyses, and precisely measuring these margins is considered intractable [14, 15].

A popular technique (which we revisit in this work) is to approximate the classification margin using a first-order Taylor approximation. Elsayed et al. [16] use this method in both the input and hidden space, and then formulate a loss function that maximizes these margins. However, while this results in a measurable increase in margin, it does not result in any significant gains in test accuracy. In a seminal paper, Jiang et al. [11] utilize the same approximation in order to predict the generalization gap of a set of trained networks by training a linear regression model on a summary of their hidden margin distributions. Natekar and Sharma [17] demonstrate that this measure can be further improved if margins are measured using the representations of Mixup [18] or augmented training samples. Similarly, Chuang et al. [6] introduce novel generalization bounds and slightly improve on this metric by proposing an alternative cluster-aware normalization scheme ( $k$ -variance [19]).

Input margins are generally considered from the point of view of adversarial robustness, and many techniques have been developed to generate adversarial samples on or near the decision boundary. Examples include: the Carlini and Wagner Attack [20], Projected Gradient Descent [21], and DeepFool [22]. Some of these studies have investigated the link between adversarial robustness and generalization, often concluding that an inherent trade-off exists [23, 24, 25]. However, this conclusion and its intricacies are still being debated [26].

Yousefzadeh and O’Leary [14] formulate finding a point on the decision boundary as a constrained minimization problem, which is solved using an off-the-shelf optimization method. While this method is more precise, it comes at a great computational cost. To alleviate this, dimensionality reduction techniques are used in the case of image data to reduce the number of input features. The same formulation was later applied in [27] without any prior dimensionality reduction, at the expense of a significant computational burden.

In this work we propose a modification to the Taylor approximation of the input classification margin (and its iterative alternative DeepFool) in order for it to be more predictive of generalization.

## 2.2 Predicting Generalization in Deep Learning

The PGDL challenge was a competition hosted at NeurIPS 2020 [8]. The objective of this challenge was to design a complexity measure to rank models according to their generalization gap. More precisely, participants only had access to a set of trained models, along with their parameters and training data, and were tasked with ranking the models within each set according to their generalization gap. Each solution was then evaluated on how well its ranking aligns with the true ranking on a held-out set of tasks, which was unknown to the competitors.

In total, there are 550 trained models across 8 different tasks and 6 different image classification datasets, where each task refers to a set of models trained on the same dataset with varying hyperparameters and subsequent test accuracy. Tasks 1, 2, 4, and 5 were available for prototyping and tuning complexity measures, while Task 6 to 9 were used as a held-out set. There is no task 3. The final average score on the test set was the only metric used to rank the competitors. Conditional mutual information (CMI) is used as evaluation metric, which measures the conditional mutual information between the complexity measure and true generalization gap, given that a set of hyperparameter types are observed. This is done in order to prevent spurious correlations resulting from specific hyperparameters, a step towards establishing whether a causal relationship exists.

All models were trained to approximately the same, near zero, training loss. Note that this implies that ranking models according to either their generalization gap or test accuracy is essentially equivalent.

Several interesting solutions were developed during the challenge: In addition to the modification of hidden margins mentioned earlier, the winning team [17] developed several prediction methods based on the internal representations of each model. Their best-performing method measures clustering characteristics of hidden layers (using Davies-Bouldin Index [28]), and combines this with the model’s accuracy on Mixup-augmented training samples. In a similar fashion, the runners-up based their metrics on measuring the robustness of trained networks to augmentations of their training data [29].

After the competition’s completion, the dataset was made publicly available, inspiring further research: Schiff et al. [30] generated perturbation response curves that ‘capture the accuracy change of a given network as a function of varying levels of training sample perturbation’ and develop statistical measures from these curves. They produced eleven complexity measures with different types of sample Mixup and statistical metrics.

While several of the methods rely on using synthetic samples (e.g. Mixup), Zhang et al. [31] take this to the extreme and generate an artificial test set using pretrained generative adversarial networks (GANs). They demonstrate that simply measuring the classification accuracy on this synthetic test set is very predictive of a model’s generalization. While practically useful, this method does not make a link between any characteristics of the model and its generalization ability.

## 3 Theoretical approach

This section provides a theoretical overview of the proposed complexity measure. We first explain our intuition surrounding classification margins, before mathematically formulating constrained margins.

### 3.1 Intuition

A correctly classified training sample with a large margin can have more varied feature values, potentially due to noise, and still be correctly classified. However, as we will show, input margins are not generally predictive of generalization. This observation is supported by literature regarding adversarial robustness, where it has been shown that adversarial retraining (which increases input margins) can negatively affect generalization [23, 25].

Stutz et al. [26] provide a plausible reason for this counter-intuitive observation: Through the use of Variational Autoencoder GANs they show that the majority of adversarial samples leave the class-specific data manifold of the samples’ class. They offer the intuitive example of black border pixels in the case of MNIST images, which are zero for all training samples. Samples found on the decision boundary which manipulate these border pixels have a zero probability under the data distribution, and they do not lie on the underlying manifold.

We leverage this intuition and argue that any input margin measure that relates to generalization should measure distances along directions that do not rely on spurious features in the input space. The intuition is that, while nearby decision boundaries exist for virtually any given training sample, these nearby decision boundaries are likely in directions which are not inherently useful for test set classification, i.e. they diverge from the underlying data manifold.

More specifically, we argue that margins should be measured in directions of ‘high utility’, that is, directions that are expected to be useful for characterising a given dataset, while ignoring those of lower utility. In our case, we approximate these directions by defining high utility directions as directions which explain a large amount of variance in the data. We extract these using Principal Component Analysis (PCA). While typically used as a dimensionality reduction technique, PCA can be interpreted as learning a low-dimensional manifold [32], albeit a locally linear one. In this way, the PCA manifold identifies subspaces that are thought to contain the variables that are truly relevant to the underlying data distribution, which the out-of-sample data is assumed to also be generated from. In the following section, we formalize such a measure.

### 3.2 Constrained Margins

We first formulate the classical definition of an input margin [14], before adapting it for our purpose.

Let  $f : X \rightarrow \mathbb{R}^{|N|}$  denote a classification model with a set of output classes  $N = \{1 \dots n\}$ , and  $f_k(\mathbf{x})$  the output value of the model for input sample  $\mathbf{x}$  and output class  $k$ .

For a correctly classified input sample  $\mathbf{x}$ , the goal is to find the closest point  $\hat{\mathbf{x}}$  on the decision boundary between the true class  $i$  (where  $i = \arg \max_k (f_k(\mathbf{x}))$ ) and another class  $j \neq i$ . Formally,  $\hat{\mathbf{x}}$  is found by solving the constrained minimization problem:

$$\arg \min_{\hat{\mathbf{x}} \in [L, U]} \|\mathbf{x} - \hat{\mathbf{x}}\|_2 \quad (1)$$

with  $L$  and  $U$  the lower and upper bounds of the search space, respectively, such that

$$f_i(\hat{\mathbf{x}}) = f_j(\hat{\mathbf{x}}) \quad (2)$$

for  $i$  and  $j$  as above.

The margin is then given by the Euclidean distance between the input sample,  $\mathbf{x}$ , and its corresponding sample on the decision boundary,  $\hat{\mathbf{x}}$ . We now adapt this definition in order to define a ‘constrained margin’. Let the set  $P = \{\mathbf{p}_1, \mathbf{p}_2, \dots, \mathbf{p}_m\}$  denote the first  $m$  principal component vectors of the training dataset, that is, the  $m$  orthogonal principal components which explain the most variance. Such principal components are straightforward to extract by calculating the eigenvectors of the covariance matrix of the normalized training data, where the data is normalized the same as prior to model training.

We now restrict  $\hat{\mathbf{x}}$  to any point consisting of the original sample  $\mathbf{x}$  plus a linear combination of these (unit length) principal component vectors, that is, for some coefficient vector  $\mathbf{B} = [\beta_1, \beta_2, \dots, \beta_m]$

$$\hat{\mathbf{x}} \triangleq \mathbf{x} + \sum_{i=1}^m \beta_i \mathbf{p}_i \quad (3)$$

Substituting  $\hat{\mathbf{x}}$  into the original objective function of Equation (1), the new objective becomes

$$\min_{\beta} \left\| \sum_{i=1}^m \beta_i \mathbf{p}_i \right\|_2 \quad (4)$$

such that Equation (2) is approximated within a certain tolerance. For this definition of margin, the search space is constrained to a lower-dimensional subspace spanned by the principal components with point  $\mathbf{x}$  as origin, and the optimization problem then simplifies to finding a point on the decision boundary within this subspace. By doing so, we ensure that boundary samples that rely on spurious features (that is, in directions of low utility) are not considered viable solutions to Equation (1). Note that this formulation does not take any class labels into account for identifying high utility directions.

While it is possible to solve the constrained minimization problem using a constrained optimizer [14], we approximate the solution by adapting the previously mentioned first-order Taylor approximation [16, 33], which greatly reduces the computational cost. The Taylor approximation of the

constrained margin  $d(\mathbf{x})$  for a sample  $\mathbf{x}$  between classes  $i$  and  $j$  when using an  $L2$  norm is given by

$$d(\mathbf{x}) = \frac{f_i(\mathbf{x}) - f_j(\mathbf{x})}{\| [\nabla_{\mathbf{x}} f_i(\mathbf{x}) - \nabla_{\mathbf{x}} f_j(\mathbf{x})] \mathbf{P}^T \|_2} \quad (5)$$

where  $\mathbf{P}$  is the  $m \times n$  matrix formed by the top  $m$  principal components with  $n$  input features.

The derivation of Equation (5) is included in the appendix (Section C).

The value  $d(\mathbf{x})$  only approximates the margin and the associated discrepancy in Equation (2) can be large. In order to reduce this to within a reasonable tolerance, we apply Equation (5) in an iterative manner, using a modification of the well-known DeepFool algorithm [22]. DeepFool was defined in the context of generating adversarial samples with the smallest possible perturbation, which is in effect very similar to finding the nearest point on the decision boundary with the smallest violation of Equation (2).

To extract the DeepFool constrained margin for some sample  $\mathbf{x}$ , the Taylor approximation of the constrained margin is calculated between the true class  $i$  and all other classes  $j$ , individually. A small step (scaled by a set learning rate) is then taken in the lower-dimensional subspace in the direction corresponding to the class with smallest margin. This point is then transformed back to the original feature space and the process is repeated until the distance changes less than a given tolerance in comparison to the previous iteration. The exact process to calculate a DeepFool constrained margin is described in Algorithm 1. Note that we also clip  $\hat{\mathbf{x}}$  according to the minimum and maximum feature values of the dataset after each step, which ensures that the point stays within the bound constraints expressed in Equation 1. While this is likely superfluous when generating normal adversarial samples – they are generally very close to the original  $\mathbf{x}$  – it is a consideration when the search space is constrained, with clipped margins performing better. (See Section A.3 in the appendix for an ablation analysis of clipping.)

---

**Algorithm 1** DeepFool constrained margin calculation

---

**Input:** Sample  $\mathbf{x}$ , classifier  $f$ , principal components  $\mathbf{P}$

**Parameter:** Stopping tolerance  $\delta$ , Learning rate  $\gamma$ , Maximum iterations  $max$

**Output:** Distance  $d_{best}$ , Equality violation  $v_{best}$

```

1:  $\hat{\mathbf{x}} \leftarrow \mathbf{x}, i \leftarrow \arg \max_k f_k(\mathbf{x}), d \leftarrow 0, v_{best} \leftarrow \infty, c \leftarrow 0$ 
2: while  $c \leq max$  do
3:   for  $j \neq i$  do
4:      $o_j \leftarrow f_i(\hat{\mathbf{x}}) - f_j(\hat{\mathbf{x}})$ 
5:      $\mathbf{w}_j \leftarrow [\nabla f_i(\hat{\mathbf{x}}) - \nabla f_j(\hat{\mathbf{x}})] \mathbf{P}^T$ 
6:   end for
7:    $l \leftarrow \arg \min_{j \neq i} \frac{|o_j|}{\|\mathbf{w}_j\|_2}$ 
8:    $\mathbf{r} \leftarrow \frac{|o_l|}{\|\mathbf{w}_l\|_2} \mathbf{w}_l \mathbf{P}$ 
9:    $\hat{\mathbf{x}} \leftarrow \hat{\mathbf{x}} + \gamma \mathbf{r}$ 
10:   $\hat{\mathbf{x}} \leftarrow \text{clip}(\hat{\mathbf{x}})$ 
11:   $v \leftarrow |o_l|$ 
12:   $d \leftarrow \|\mathbf{x} - \hat{\mathbf{x}}\|_2$ 
13:  if  $v \geq v_{best}$  or  $|d - d_{best}| < \delta$  then
14:    return  $d_{best}, v_{best}$ 
15:  else
16:     $v_{best} \leftarrow v$ 
17:     $d_{best} \leftarrow d$ 
18:     $c \leftarrow c + 1$ 
19:  end if
20: end while
21: return  $d_{best}, v_{best}$ 

```

---

## 4 Results

We investigate the extent to which constrained margins are predictive of generalization by comparing the new method with current alternatives. In Section 4.1 we describe our experimental setup.

Following this, we do a careful comparison between our metric and existing techniques based on standard input and hidden margins (Section 4.2) and, finally, we compare with other complexity measures (Section 4.3).

#### 4.1 Experimental setup

For all margin-based measures our indicator of generalization (complexity measure) is the mean margin over 5 000 randomly selected training samples, or alternatively the maximum number available for tasks with less than 5 000 training samples. Only correctly classified samples are considered, and the same training samples are used for all models of the same task. To compare constrained margins to input and hidden margins we rank the model test accuracies according to the resulting indicator and calculate the Kendall’s rank correlation [34], as used in [35]. This allows for a more interpretable comparison than CMI. (As CMI is used throughout the PGDL challenge, we also include the resulting CMI scores in Section B of the appendix.) To compare constrained margins to published results of other complexity measures, we measure CMI between the complexity measure and generalization gap and contrast this with the reported scores of other methods.

As a baseline we calculate the **standard input margins** (‘Input’) using the first order Taylor approximation (Equation 5 without the subspace transformation), as we find that it achieves better results than the iterative DeepFool variant and is therefore the stronger baseline; see the appendix (Section B) for a full comparison.

**Hidden margins** (‘Hidden’) are measured by considering the output (post activation function) of some hidden layer, and then calculating the margin at this representation. This raises the question of which hidden layers to consider for the final complexity measure. Jiang et al. [11] consider three equally spaced layers, Natekar and Sharma [17] consider all layers, and Chuang et al. [6] consider either the first or last layer only. We calculate the mean hidden margin (using the Taylor approximation) for all these variations and find that for the tasks studied here, using the first layer performs best, while the mean over all layers comes in second. We include both results here. (A full analysis is included in Section B of the appendix.) We normalize each layer’s margin distribution by following [11], and divide each margin by the total feature variance at that layer.

Our **constrained margin** complexity measure (‘Constrained’) is obtained using Algorithm 1, although in practice we implement this in a batched manner. Empirically, we find that the technique is not very sensitive with regard to the selection of hyperparameters and a single learning rate ( $\gamma = 0.25$ ), tolerance ( $\delta = 0.01$ ), and max iterations ( $max = 100$ ) is used across all experiments. The number of principal components for each dataset is selected by plotting the explained variance (of the train data) per principal component in decreasing order on a logarithmic scale and applying the elbow method using the Kneedle algorithm from Satopaa et al [36]. This results in a very low-dimensional search space, ranging from 3 to 8 principal components for the seven unique datasets considered.

In order to prevent biasing our metric to the PGDL test set (tasks 6 to 9) we did not perform any tuning or development of the complexity measure using these tasks, nor do we tune any hyperparameters per task. The choice of principal component selection algorithm was done after a careful analysis of Tasks 1 to 5 only, see additional details in the appendix (A.1). In terms of computational expense, we find that calculating the entire constrained margin distribution only takes 1 to 2 minutes per model on an Nvidia A30.

#### 4.2 Margin complexity measures

In Table 1 we show the Kendall’s rank correlation obtained when ranking models according to constrained margin, standard input margins, and hidden margins. It can be observed that standard input margins are not predictive of generalization for most tasks and, in fact, show a negative correlation for some. This unstable behaviour is supported by ongoing work surrounding adversarial robustness and generalization [23, 24, 25]. Furthermore, we observe a very large performance gap between constrained and standard input margins, and an increase from 0.24 to 0.66 average rank correlation is observed by constraining the margin search. This strongly supports our initial intuitions.

In the case of hidden margins, performance is more competitive, however, constrained margins still outperform hidden margins on 6 out of 8 tasks. One also observes that the selection of hidden layers can have a very large effect, and the discrepancy between the two hidden-layer selections is

Table 1: Kendall’s rank correlation between mean margin and test accuracy for constrained, standard input, and hidden margins using the first or all layer(s). Models in Task 4 are trained with batch normalization while models in Task 5 are trained without. There is no Task 3.

Task	Architecture	Dataset	Constrained	Input	Hidden (1st)	Hidden (all)
1	VGG	CIFAR10	<b>0.8040</b>	0.0265	0.5794	0.7825
2	NiN	SVHN	<b>0.8672</b>	0.6841	0.7037	0.8281
4	FCN	CINIC10	0.6651	0.6251	<b>0.7958</b>	0.2707
5	FCN	CINIC10	0.2292	0.3571	<b>0.5427</b>	0.1329
6	NiN	OxFlowers	<b>0.8008</b>	-0.1351	0.4427	0.2839
7	NiN	OxPets	<b>0.5027</b>	0.3215	0.3623	0.3925
8	VGG	FMNIST	<b>0.6004</b>	-0.1233	-0.0656	0.1859
9	NiN	CIFAR10 (augmented)	<b>0.8145</b>	0.1573	0.7097	0.4556
Average			<b>0.6605</b>	0.2392	0.5088	0.4165

significant. Given that our constrained margin measurement is limited to the input space, there are several advantages: 1) no normalization is required, as all models share the same input space, and 2) the method is more robust when comparing models with varying topology, as no specific layers need to be selected.

### 4.3 Other complexity measures

To further assess the predictive power of constrained margins, we compare our method to the reported CMI scores of several other complexity measures. We compare against three solutions from the winning team [17], as well as the best solutions from two more recent works [6, 30], where that of Schiff et al. [30] has the highest average test set performance we are aware of. We do not compare against pretrained GANs [31]. The original naming of each method is kept. Of particular relevance are the *MM* and *AM* columns, which are hidden margins applied to Mixup and Augmented samples, as well as *kV*-Margin and *kV*-GN-Margin which are output and hidden margins with *k*-Variance normalization, respectively. The results of this comparison are shown in Table 2.

One observes that constrained margins achieve highly competitive scores, and in fact, outperform all other measures on 4 out of 8 tasks. It is also important to note that the *MM* and *AM* columns show that hidden margins can be improved in some cases if they are measured using the representations of Mixup or augmented training samples. That said, these methods still underperform on average in comparison to constrained input margins, which do not rely on any form of data augmentation.

Table 2: Conditional Mutual Information (CMI) scores for several complexity measures on the PGDL dataset. Acronyms: *DBI*=Davies Bouldin Index, *LWM*=Label-wise Mixup, *MM*=Mixup Margins, *AM*=Augmented Margins, *kV*=*k*-Variance, *GN*=Gradient Normalized, *Gi*=Gini coefficient, *Mi*=Mixup. Test set average is the average over tasks 6 to 9. There is no Task 3. †Indicates a margin-based measure.

Task	Natekar and Sharma			Chuang et al.		Schiff et al.	Ours
	DBI*LWM	MM†	AM†	<i>kV</i> -Margin 1st†	<i>kV</i> -GN-Margin 1st†	PCA Gi&Mi	Constrained Margin†
1	00.00	01.11	05.73	05.34	17.95	0.04	<b>39.37</b>
2	32.05	47.33	44.60	26.78	44.57	38.08	<b>51.12</b>
4	31.79	43.22	<b>47.22</b>	37.00	30.61	33.76	21.48
5	15.92	<b>34.57</b>	22.82	16.93	16.02	20.33	05.12
6	<b>43.99</b>	11.46	08.67	06.26	04.48	40.06	30.52
7	12.59	<b>21.98</b>	11.97	02.07	03.92	13.19	12.60
8	09.24	01.48	01.28	01.82	00.61	10.30	<b>13.54</b>
9	25.86	20.78	15.25	15.75	21.20	33.16	<b>51.46</b>
Test set average	22.92	13.93	09.29	06.48	07.55	23.62	<b>27.03</b>

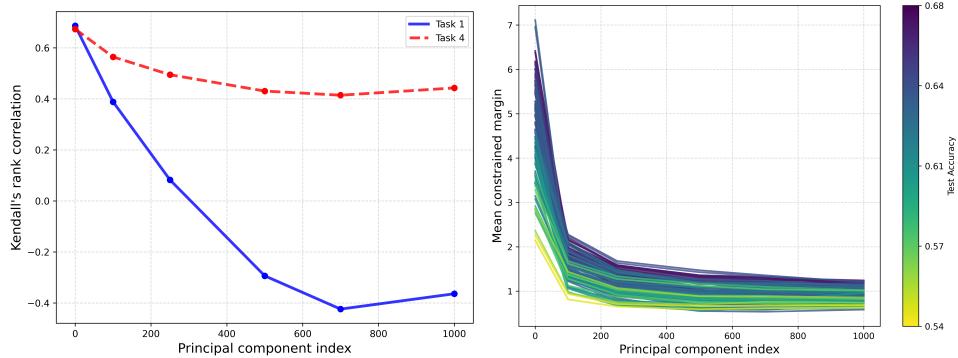


Figure 1: Comparison of high to low utility directions using subspaces spanned by 10 principal components, x-axis indicates the first component in each set of principal components. Left: Kendall’s rank correlation for Task 1 (blue solid line) and 4 (red dashed line). Right: Mean constrained margin for models from Task 4.

## 5 A closer look

In this section we do a further analysis of constrained margins. In Section 5.1 we investigate how the performance of constrained margins changes when lower utility subspaces are considered, whereafter we discuss limitations of the method in Section 5.2.

### 5.1 High to low utility

We examine how high utility directions compare to those of lower utility when calculating constrained margins. This allows us to further test our approach, as one would expect that margins measured using the lower-ranked principal components should be less predictive of a model’s performance.

We calculate the mean constrained margin using select subsets of 10 contiguous principal components in descending order of explained variance. For example, we calculate the constrained margins using components 1 to 10, then 100 to 109, etc. This allows us to calculate the distance to the decision boundary using 10 dimensional subspaces of decreasing utility. We, once again, make use of 5 000 training samples. We restrict ourselves to analysing the training set of tasks (tasks 1-5) and consider one task where constrained margins perform very well (Task 1) and one with poorer performance (Task 4). Figure 1 (left) shows the resulting Kendall’s rank correlation for each subset of principal components indexed by the first component in each set (principal component index). The right-hand side shows the mean margin of all models from Task 4 at each subset.

As expected, the first principal components lead to margins that are more predictive of generalization. We see a gradual decrease in predictive power when considering later principal components. Task 1 especially suffers this phenomenon, reaching negative correlations. This supports the idea that utilizing the directions of highest utility is a necessary aspect of input margin measurements. Additionally, one observes that the mean margin also rapidly decreases after the first few sets of principal components. After the point shown here (index 1 000), we find that the mean margin increases as DeepFool struggles to find samples on the decision boundary within the bound constraints. Due to this, it is difficult to draw any conclusions from an investigation of the lower-ranked principal components. This also points to the notion that the adversarial vulnerability of modern DNNs is in part due to nearby decision boundaries in the directions of the mid-tier principal components (the range of 100 to 1 000).

### 5.2 Limitations

It has been demonstrated that our proposed metric performs well and aligns with our initial intuition. However, there are also certain limitations that require explanation. Empirically we observe that, for tasks where constrained margins perform well, they do so across all hyperparameter variations, with the exception of depth. This is illustrated in Figure 2 (left), which shows the mean constrained margin versus test accuracy for Task 1. We observe that sets of networks with two and six convolutional



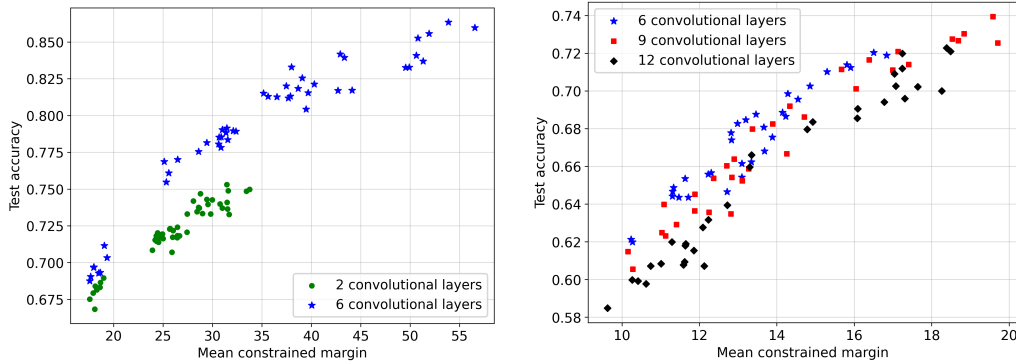


Figure 2: Mean constrained margin versus test accuracy for PGDL Task 1 (left) and 6 (right). Left: Models with 2 (green circle) and 6 (blue star) convolutional layers. Right: Models with 6 (blue star), 9 (red square), and 12 (black diamond) convolutional layers.

layers, respectively, each exhibit a separate relationship between margin and test accuracy. This discrepancy is not always as strongly present: for Task 6 all three depth configurations show a more similar relationship, as observed on the right of Figure 2, although the discrepancy is still present. The same trend holds for all tasks where it is observed (1, 2, 4, 6, 9). It appears that shallower networks model the input space in a distinctly different fashion than their deeper counterparts. For tasks such as 5 and 7, where constrained margins perform more poorly, there is no single hyperparameter that appears to be the culprit. We do note that the resulting scatter plots of margin versus test accuracy never show points in the lower right (large margin but low generalization) or upper left (small margin but high generalization) quadrants. It is therefore possible that a larger constrained margin is always beneficial to a model’s generalization, even though it is not always fully descriptive of its performance. Finally, while our approach to selecting the number of principal components is experimentally sound, the results can be further improved if the optimal number is known, see Section A.1 in the appendix for details.

## 6 Conclusion

We have shown that constraining input margins to high utility subspaces can significantly improve their predictive power i.t.o generalization. Specifically, we have used the principal components of the data as a proxy for identifying these subspaces, which can be considered a rough approximation of the underlying data manifold.

Constraining the search to a warped subspace and using Euclidean distance to measure closeness is equivalent to defining a new distance metric on the original space. We are therefore, in effect, seeking a relevant distance metric to measure the closeness of the decision boundary. Understanding the requirements for such a metric remains an open question. Unfortunately, current approximations and methods for finding points on the decision boundary are largely confined to  $L_p$  metrics. The positive results achieved with the current PCA-and-Euclidean-based approach provide strong motivation that this is a useful avenue to pursue.

Furthermore, we believe that constrained margins can be used as a tool to further probe generalization, similar to the large amount of work that has been done surrounding standard input margins and characterization of decision boundaries.

In conclusion, we propose constraining input margins to make them more predictive of generalization in DNNs. It has been demonstrated that this greatly increases the predictive power of input margins, and also outperforms hidden margins and several other contemporary methods on the PGDL tasks. This method has the benefits of requiring no per-layer normalization, no arbitrary selection of hidden layers, and does not rely on any form of surrogate test set (e.g. data augmentation or synthetic samples).

## References

- [1] Vladimir N Vapnik. An overview of statistical learning theory. *IEEE Transactions on Neural Networks*, 10(5):988–999, 1999.
- [2] Vladimir Koltchinskii and Dmitry Panchenko. Empirical margin distributions and bounding the generalization error of combined classifiers. *The Annals of Statistics*, 30(1):1–50, 2002.
- [3] Chiyuan Zhang, Samy Bengio, Moritz Hardt, Benjamin Recht, and Oriol Vinyals. Understanding deep learning (still) requires rethinking generalization. *Communications of the ACM*, 64(3):107–115, 2021.
- [4] Sanjeev Arora, Rong Ge, Behnam Neyshabur, and Yi Zhang. Stronger generalization bounds for deep nets via a compression approach. In *International Conference on Machine Learning (ICML)*, pages 254–263. PMLR, 2018.
- [5] Kenji Kawaguchi, Leslie Pack Kaelbling, and Yoshua Bengio. *Generalization in Deep Learning. Mathematical Aspects of Deep Learning*. Cambridge University Press, 2022.
- [6] Ching-Yao Chuang, Youssef Mroueh, Kristjan Greenewald, Antonio Torralba, and Stefanie Jegelka. Measuring generalization with optimal transport. *Advances in Neural Information Processing Systems*, 34:8294–8306, 2021.
- [7] Sanae Lotfi, Marc Anton Finzi, Sanyam Kapoor, Andres Potapczynski, Micah Goldblum, and Andrew Gordon Wilson. PAC-Bayes compression bounds so tight that they can explain generalization. In *Advances in Neural Information Processing Systems*, 2022.
- [8] Yiding Jiang, Pierre Foret, Scott Yak, Daniel M Roy, Hossein Mobahi, Gintare Karolina Dziugaite, Samy Bengio, Suriya Gunasekar, Isabelle Guyon, and Behnam Neyshabur. Neurips 2020 competition: Predicting generalization in deep learning. *arXiv preprint arXiv:2012.07976*, 2020.
- [9] Peter L Bartlett, Dylan J Foster, and Matus J Telgarsky. Spectrally-normalized margin bounds for neural networks. *Advances in Neural Information Processing Systems*, 30, 2017.
- [10] Jure Sokolić, Raja Giryes, Guillermo Sapiro, and Miguel RD Rodrigues. Robust large margin deep neural networks. *IEEE Transactions on Signal Processing*, 65(16):4265–4280, 2017.
- [11] Yiding Jiang, Dilip Krishnan, Hossein Mobahi, and Samy Bengio. Predicting the generalization gap in deep networks with margin distributions. In *International Conference on Learning Representations*, 2018.
- [12] Bernhard E Boser, Isabelle M Guyon, and Vladimir N Vapnik. A training algorithm for optimal margin classifiers. In *Proceedings of the fifth annual workshop on Computational Learning Theory*, pages 144–152, 1992.
- [13] Kilian Q. Weinberger and Lawrence K. Saul. Distance metric learning for large margin nearest neighbor classification. *Journal of Machine Learning Research*, 10(9):207–244, 2009.
- [14] Roozbeh Yousefzadeh and Dianne P. O’Leary. Deep learning interpretation: Flip points and homotopy methods. In Jianfeng Lu and Rachel Ward, editors, *Proceedings of The First Mathematical and Scientific Machine Learning Conference*, volume 107 of *Proceedings of Machine Learning Research*, pages 1–26. PMLR, 20–24 Jul 2020.
- [15] Yaoqing Yang, Rajiv Khanna, Yaodong Yu, Amir Gholami, Kurt Keutzer, Joseph E Gonzalez, Kannan Ramchandran, and Michael W Mahoney. Boundary thickness and robustness in learning models. *Advances in Neural Information Processing Systems*, 33:6223–6234, 2020.
- [16] Gamaleldin Elsayed, Dilip Krishnan, Hossein Mobahi, Kevin Regan, and Samy Bengio. Large margin deep networks for classification. *Advances in Neural Information Processing Systems*, 31, 2018.
- [17] Parth Natekar and Manik Sharma. Representation based complexity measures for predicting generalization in deep learning. *arXiv preprint arXiv:2012.02775*, 2020.
- [18] Hongyi Zhang, Moustapha Cisse, Yann N. Dauphin, and David Lopez-Paz. mixup: Beyond empirical risk minimization. In *International Conference on Learning Representations*, 2018.
- [19] Justin Solomon, Kristjan Greenewald, and Haikady Nagaraja. k-variance: A clustered notion of variance. *SIAM Journal on Mathematics of Data Science*, 4(3):957–978, 2022.

- [20] Nicholas Carlini and David Wagner. Towards evaluating the robustness of neural networks. In *IEEE Symposium on Security and Privacy*, pages 39–57. IEEE, 2017.
- [21] Aleksander Madry, Aleksandar Makelov, Ludwig Schmidt, Dimitris Tsipras, and Adrian Vladu. Towards deep learning models resistant to adversarial attacks. In *International Conference on Learning Representations*, 2018.
- [22] Seyed-Mohsen Moosavi-Dezfooli, Alhussein Fawzi, and Pascal Frossard. DeepFool: a simple and accurate method to fool deep neural networks. In *Proceedings of the IEEE Conference on Computer Vision and Pattern Recognition*, pages 2574–2582, 2016.
- [23] Dimitris Tsipras, Shibani Santurkar, Logan Engstrom, Alexander Turner, and Aleksander Madry. Robustness May Be at Odds with Accuracy. In *International Conference on Learning Representations*, 2019.
- [24] Dong Su, Huan Zhang, Hongge Chen, Jinfeng Yi, Pin-Yu Chen, and Yupeng Gao. Is Robustness the Cost of Accuracy?—A Comprehensive Study on the Robustness of 18 Deep Image Classification Models. In *Proceedings of the European Conference on Computer Vision (ECCV)*, pages 631–648, 2018.
- [25] Aditi Raghunathan, Sang Michael Xie, Fanny Yang, John Duchi, and Percy Liang. Adversarial Training Can Hurt Generalization. In *ICML Workshop on Identifying and Understanding Deep Learning Phenomena*, 2019.
- [26] David Stutz, Matthias Hein, and Bernt Schiele. Disentangling Adversarial Robustness and Generalization. In *Proceedings of the IEEE/CVF Conference on Computer Vision and Pattern Recognition*, pages 6976–6987, 2019.
- [27] Marthinus Wilhelmus Theunissen, Coenraad Mouton, and Marelle H Davel. The Missing Margin: How Sample Corruption Affects Distance to the Boundary in ANNs. In *Southern African Conference for Artificial Intelligence Research*, pages 78–92. Springer, 2022.
- [28] David L Davies and Donald W Bouldin. A cluster separation measure. *IEEE Transactions on Pattern Analysis and Machine Intelligence*, (2):224–227, 1979.
- [29] Dhruva Kashyap, Natarajan Subramanyam, et al. Robustness to augmentations as a generalization metric. *arXiv preprint arXiv:2101.06459*, 2021.
- [30] Yair Schiff, Brian Quanz, Payel Das, and Pin-Yu Chen. Predicting Deep Neural Network Generalization with Perturbation Response Curves. *Advances in Neural Information Processing Systems*, 34:21176–21188, 2021.
- [31] Yi Zhang, Arushi Gupta, Nikunj Saunshi, and Sanjeev Arora. On Predicting Generalization using GANs. In *International Conference on Learning Representations*, 2022.
- [32] Geoffrey E Hinton, Peter Dayan, and Michael Revow. Modeling the Manifolds of Images of Handwritten Digits. *IEEE Transactions on Neural Networks*, 8(1):65–74, 1997.
- [33] Ruitong Huang, Bing Xu, Dale Schuurmans, and Csaba Szepesvári. Learning with a Strong Adversary. *arXiv preprint arXiv:1511.03034*, 2015.
- [34] M. G. Kendall. A New Measure of Rank Correlation. *Biometrika*, 30(1-2):81–93, 06 1938.
- [35] Yiding Jiang, Behnam Neyshabur, Hossein Mobahi, Dilip Krishnan, and Samy Bengio. Fantastic generalization measures and where to find them. In *International Conference on Learning Representations*, 2019.
- [36] Ville Satopaa, Jeannie Albrecht, David Irwin, and Barath Raghavan. Finding a "kneeder" in a haystack: Detecting knee points in system behavior. In *2011 31st international Conference on Distributed Computing systems workshops*, pages 166–171. IEEE, 2011.

## A Constrained margin ablation

This section demonstrates the effect of several hyperparameters on the performance of constrained margins. We analyse the selection of the number of principal components, the number of samples, as well as the effect of clipping.

### A.1 Number of principal components

In order to better understand the interaction between the selection of the number of principal components and predictive power, we calculate the mean constrained margin using 1 to 50 principal components for all the development set tasks (tasks 1 to 5). We once again make use of 5 000 samples. However, in this case, the first order Taylor approximation is used to reduce the computational burden. The result of this analysis is shown in Figure 3. We indicate the number of principal components selected by the Kneedle algorithm [36] (applied to the principal components in descending order of explained variance) for each task with a star.

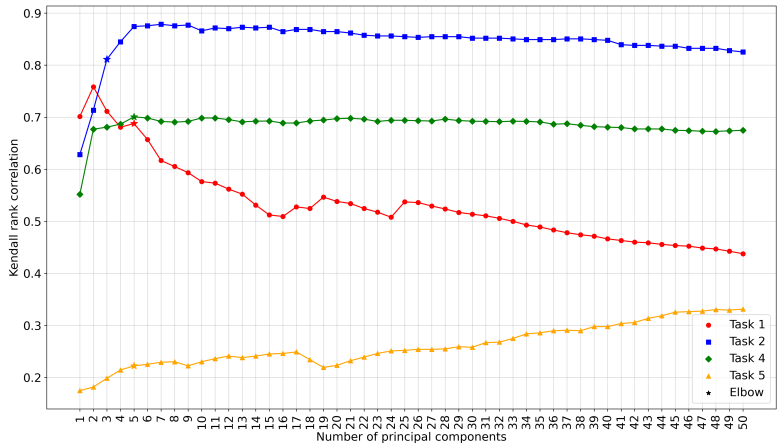


Figure 3: Predictive performance (Kendall’s rank correlation) as a function of the number of principal components for Task 1 (red circles), 2 (blue squares), 4 (green diamonds), and 5 (yellow triangles). The number of principal components reported on per task in the main paper is indicated with a star.

One observes that the elbow method selects the number of components in a near-optimal fashion for Task 1, 2, and 4. Furthermore, the optimal number is generally very low, whereafter the correlation decreases. Task 5 (which is the task for which constrained margins produce the lowest performance) behaves in a contrary manner, as the ranking correlation increases as the number of components becomes larger. We find that it only reaches a maximum rank correlation of 0.4 at 270 components (not shown here).

In Section 5.1 we had compared the predictive performance of using subspaces of decreasing utility to calculate constrained margins. We now repeat this experiment, but rather increase the size of the subspace up to its maximum (the dimensionality of the input data). This allows us to further verify whether our method of selecting the number of principal components is sound. The result of this analysis is shown in Figure 4 for tasks 1 and 4.

One observes that the predictive ability of the constrained margin metric decreases as the size of the subspace is increased until it reaches that of standard input margins, which is well aligned with what one would expect.

### A.2 Number of samples

We have used 5 000 samples to calculate the mean constrained margin for each task (and the same number for all other margin measurements). It is worth determining what effect the number of samples has on the final performance. In Figure 5 we show the Kendall’s rank correlation between

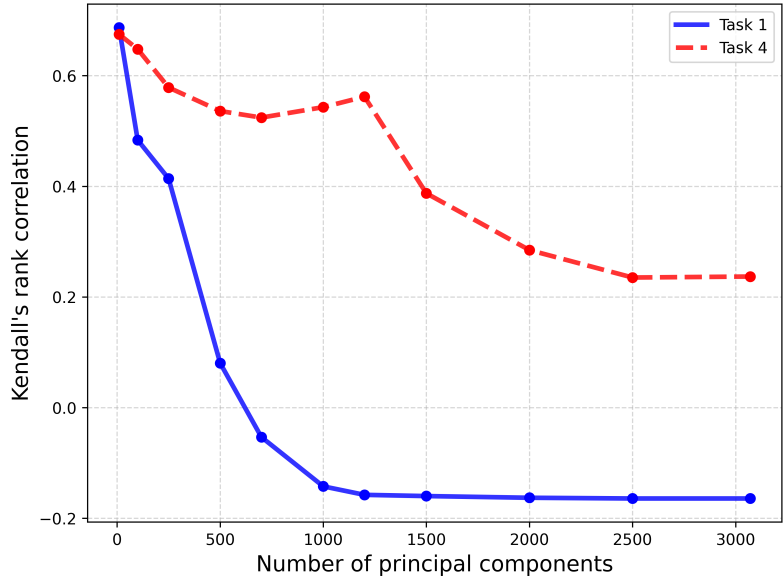


Figure 4: Predictive performance (Kendall’s rank correlation) of constrained margin as a function of the number of principal components for Task 1 (blue solid line) and 4 (red dashed line) calculated using Algorithm (1).

mean constrained margin and test accuracy for the development set using 500 to 5 000 samples (using the modified DeepFool algorithm).

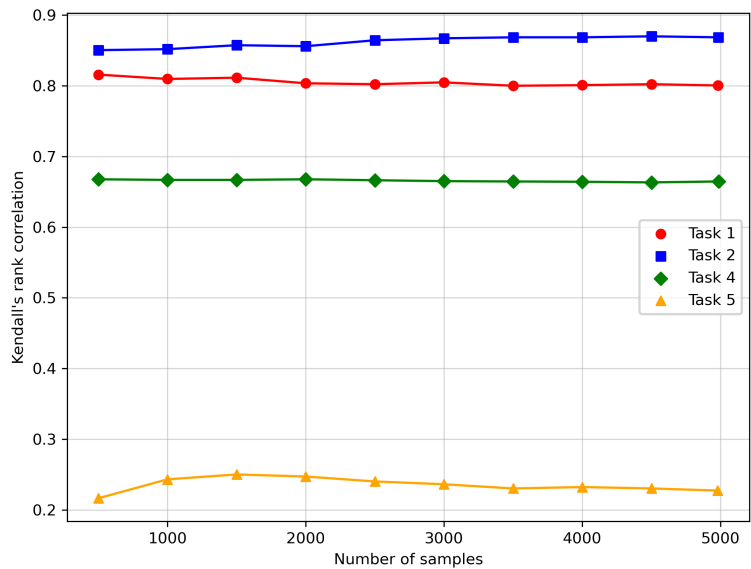


Figure 5: Predictive performance of constrained margins (Kendall’s rank correlation) as a function of the number of principal components for Task 1 (red circles), 2 (blue squares), 4 (green diamonds), and 5 (yellow triangles).

One observes that the rank correlation plateaus rather quickly for most tasks, and one can likely get away with only using 500 to 1 000 samples per model. However, to mitigate any effect that the stochastic selection of training samples can have on the reproducibility of the results, we have chosen

to use 5 000 throughout. To this end, we show the number of principal components selected, as well as the number of samples used for each task in Table 3, note that Task 6 and 7 use the maximum number of samples available.

Table 3: Number of principal components and samples used for each task to calculate constrained margins. Tasks 6 and 7 use the maximum number of samples available for the dataset.

Task	Dataset	Components	Samples
1	CIFAR10	5	5 000
2	SVHN	3	5 000
4	CINIC10	5	5 000
5	CINIC10	5	5 000
6	OxFlowers	8	2 040
7	OxPets	3	3 680
8	FMNIST	4	5 000
9	CIFAR10 (augmented)	5	5 000

### A.3 Enforcing bound constraints

Our modified DeepFool algorithm (Algorithm 1 in the main paper) enforces bound constraints on the sample by clipping  $\hat{x}$  to stay within the minimum and maximum feature values of the dataset after each step (see line 10 of the algorithm). Since the original images have pixel values between 0 and 1, the z-normalised data has a strict lower and upper bound. Allowing  $\hat{x}$  to deviate outside these values will produce boundaries that cannot exist in practice. Given that the original DeepFool algorithm does not include any form of bound constraints, we analyse the effect clipping has on the performance of constrained and standard input margins. Table 4 shows the Kendall’s rank correlation per task with and without clipping.

Table 4: Kendall’s rank correlation between mean margin and test accuracy for constrained and standard input margins with and without clipping.

Task	Constrained		Input	
	Clipped	Unclipped	Clipped	Unclipped
1	0.8040	<b>0.8088</b>	<b>-0.1235</b>	-0.1239
2	<b>0.8672</b>	0.8463	<b>0.6730</b>	0.6716
4	<b>0.6651</b>	0.6576	<b>0.2224</b>	0.2163
5	<b>0.2292</b>	0.1984	<b>-0.0367</b>	-0.0655
6	<b>0.8008</b>	0.7990	<b>-0.2190</b>	-0.2194
7	0.5027	<b>0.5133</b>	0.3144	<b>0.3162</b>
8	<b>0.6004</b>	0.4672	-0.1849	<b>-0.1521</b>
9	<b>0.8145</b>	0.8024	<b>0.1089</b>	0.1048
Average	<b>0.6605</b>	0.6366	<b>0.0943</b>	0.0935

It is evident that clipping has little effect on standard input margins – this makes sense, given that samples on the decision boundary are generally very close to the training sample. However, in the case of constrained margins, we observe that clipping improves the results in most cases, and especially so for Task 8. This demonstrates that enforcing the bound constraints is a useful inclusion.

## B Extended margin comparison

This section contains additional results relevant to Section 4.2 in the main paper. We compare using the first-order Taylor approximation to DeepFool, and also the selection of hidden layers.

### B.1 Comparison of Taylor and DeepFool

For constrained and standard input margins, we have experimented with using both the first-order Taylor approximation as well as the DeepFool method to calculate the distance to the decision

boundary. Here we do a full comparison between the different methods. Tables 5 and 6 show the predictive performance of all the variations using Kendall’s rank correlation and CMI, respectively.

Table 5: Kendall’s rank correlation between mean margin and test accuracy for constrained, standard input, and hidden margins for the PGDL dataset. DF indicates margins calculated using the DeepFool algorithm, while Taylor indicates the first-order Taylor approximation.

Task	Constrained (DF)	Constrained (Taylor)	Input (DF)	Input (Taylor)	Hidden 1st (Taylor)	Hidden all (Taylor)
1	<b>0.8040</b>	0.6991	-0.1235	0.0265	0.5794	0.7825
2	<b>0.8672</b>	0.8281	0.6730	0.6841	0.7037	0.8281
4	0.6651	0.6966	0.2224	0.6251	<b>0.7958</b>	0.2707
5	0.2292	0.2381	-0.0367	0.3571	<b>0.5427</b>	0.1329
6	<b>0.8008</b>	0.6753	-0.2190	-0.1351	0.4427	0.2839
7	<b>0.5027</b>	0.4192	0.3144	0.3215	0.3623	0.3925
8	<b>0.6004</b>	0.3419	-0.1849	-0.1233	-0.0656	0.1859
9	<b>0.8145</b>	0.7258	0.1089	0.1573	0.7097	0.4556
Average	<b>0.6605</b>	0.5780	0.0943	0.2392	0.5088	0.4165

Table 6: Conditional Mutual Information between mean margin and generalization gap for constrained, standard input, and hidden margins for the PGDL dataset. DF indicates margins calculated using the DeepFool algorithm, while Taylor indicates the first-order Taylor approximation.

Task	Constrained (DF)	Constrained (Taylor)	Input (DF)	Input (Taylor)	Hidden 1st (Taylor)	Hidden all (Taylor)
1	<b>39.37</b>	23.77	01.36	00.07	09.40	29.78
2	<b>51.12</b>	43.37	05.01	06.12	37.74	32.23
4	21.48	22.18	03.49	14.95	<b>34.73</b>	00.79
5	05.12	05.42	00.73	08.46	<b>19.11</b>	01.55
6	<b>30.52</b>	10.65	01.77	00.57	04.24	01.36
7	12.60	<b>12.91</b>	02.16	01.47	05.04	05.62
8	<b>13.54</b>	03.70	00.68	00.70	00.36	00.91
9	<b>51.46</b>	18.61	00.80	00.29	23.74	04.75
Average	<b>28.15</b>	17.58	02.00	04.08	16.80	09.62

One observes that constrained margins are significantly improved if the more accurate DeepFool method is applied, while standard input margins actually perform worse when using DeepFool. Due to the high dimensionality of hidden layers, it is computationally infeasible to apply DeepFool to hidden margins. However, note that constrained margins calculated using the Taylor approximation still outperform hidden margins calculated using the Taylor approximation.

## B.2 Comparison of hidden-layer selection

As mentioned in Section 4.1, there are three different methods that have previously been used to select relevant hidden layers when calculating hidden margins. In Table 7 we compare all variations: Using only the first (‘First’) or last (‘Last’) layer [6], the average margin over three equally spaced layers (‘Equally spaced’) [11], and average over all layers (‘All’) [17].

Table 7: Kendall’s rank correlation between mean hidden margin and test accuracy using different hidden layer selections.

Task	First	Last	Equally spaced	All
1	0.5794	<b>0.8294</b>	0.797	0.7825
2	0.7037	0.7135	0.775	<b>0.8281</b>
4	<b>0.7958</b>	0.1066	0.1781	0.2707
5	<b>0.5427</b>	0.0089	0.119	0.1329
6	<b>0.4427</b>	0.2365	0.2637	0.2839
7	0.3623	0.3179	0.325	<b>0.3925</b>
8	-0.0656	<b>0.2068</b>	0.0934	0.1859
9	<b>0.7097</b>	0.3831	0.4274	0.4556
Average	<b>0.5088</b>	0.3503	0.3723	0.4165

It is clear that the selection of hidden layers plays a significant role in the overall performance of hidden margins, and we observe a large variation per task between the different methods. While we have used the two best-performing methods as a benchmark to compare with in the main paper (‘First’ and ‘All’), this biases the comparison in favour of hidden margins, as there is no method at present to determine a priori which hidden layer selection will perform best for a given task.

### C Derivation of constrained margins (Equation (5))

This section uses the same notation as defined in Section 3.2 of the main paper. We first describe the standard linear approximation of the margin following Huang et al. [32], before deriving the constrained margin of Equation (5) as numbered in the main paper.

Any function  $f$  can be approximated with its differential at point  $\mathbf{x}$  using

$$\hat{f}(\mathbf{x} + \mathbf{d}) = f(\mathbf{x}) + H\mathbf{d} \quad (6)$$

$$\text{where } H = \nabla_{\mathbf{x}}f(\mathbf{x}) \quad (7)$$

that is, the Jacobian of the output with regard to the input features at point  $\mathbf{x}$ . We aim to find the smallest  $\|\mathbf{d}\|$  for some norm  $\|\cdot\|$  such that  $f(\mathbf{x}) \neq f(\mathbf{x} + \mathbf{d})$ , or

$$f_j(\mathbf{x} + \mathbf{d}) \geq f_i(\mathbf{x} + \mathbf{d}) \quad (8)$$

If we approximate  $f(\cdot)$  with  $\hat{f}(\cdot)$ , this implies:

$$\begin{aligned} f_j(\mathbf{x}) + \nabla_{\mathbf{x}}f_j(\mathbf{x}) \cdot \mathbf{d} &\geq f_i(\mathbf{x}) + \nabla_{\mathbf{x}}f_i(\mathbf{x}) \cdot \mathbf{d} \\ \implies (\nabla_{\mathbf{x}}f_j(\mathbf{x}) - \nabla_{\mathbf{x}}f_i(\mathbf{x})) \cdot \mathbf{d} &\geq f_i(\mathbf{x}) - f_j(\mathbf{x}) \end{aligned} \quad (9)$$

where  $\nabla_{\mathbf{x}}f_k(\mathbf{x})$  is the gradient vector of the  $k^{th}$  output value of  $f$  with regard to input  $\mathbf{x}$ . Then, as shown in [32], the maximum  $\|\mathbf{d}\|$  will be at:

$$\|\mathbf{d}\| = \frac{f_i(\mathbf{x}) - f_j(\mathbf{x})}{\|\nabla_{\mathbf{x}}f_j(\mathbf{x}) - \nabla_{\mathbf{x}}f_i(\mathbf{x})\|_*} \quad (10)$$

where  $\|\cdot\|$  and  $\|\cdot\|_*$  are dual norms. Specifically, if  $\|\cdot\|$  is the  $L2$  norm, then:

$$\mathbf{d} = \frac{f_i(\mathbf{x}) - f_j(\mathbf{x})}{\|\nabla_{\mathbf{x}}f_j(\mathbf{x}) - \nabla_{\mathbf{x}}f_i(\mathbf{x})\|_2^2} (\nabla_{\mathbf{x}}f_j(\mathbf{x}) - \nabla_{\mathbf{x}}f_i(\mathbf{x})) \quad (11)$$

$$\text{and } \|\mathbf{d}\|_2 = \frac{f_i(\mathbf{x}) - f_j(\mathbf{x})}{\|\nabla_{\mathbf{x}}f_j(\mathbf{x}) - \nabla_{\mathbf{x}}f_i(\mathbf{x})\|_2} \quad (12)$$

Equations (11) and (12) provide the standard linear approximation of the margin as used by various authors [11, 16].

The derivation process for constrained margins is identical – it is only the calculation of the Jacobian that differs, as the gradient is calculated with regard to the transformed features rather than the



original features. Note that the size and direction of the update are calculated with regard to the transformed features but the actual step is given in the original feature space.

Let  $P_m$  be the matrix constructed from the first  $m$  principal components as column vectors:

$$P_m = [\mathbf{p}_1, \mathbf{p}_2, \dots, \mathbf{p}_m]^T \quad (13)$$

The new parameterisation  $\mathbf{x}'$  of any point  $\mathbf{x}$  is then approximated by:

$$\mathbf{x}' = P_m \mathbf{x} \quad (14)$$

where  $\mathbf{x}$  is a column vector. Let  $B_m$  be the pseudoinverse of  $P_m$ . Since the full  $P_N$ , when all components are selected, is orthogonal,  $(P_N)^{-1} = (P_N)^T$  and  $B_m$  then equals the first  $m$  rows of  $(P_N)^T$ . Then we can express each individual term  $x_k$  in terms of the elements of  $\mathbf{x}'$ :

$$x_k \approx \sum_s b_{k,s} x'_s = \sum_s p_{s,k} x'_s \quad (15)$$

with  $b_{r,c}$  the element in  $B_m$  at row  $r$  and column  $c$ , and  $p_{r,c}$  at the same position in  $P_m$ .

Let the Jacobian as used in Equations (6) to (12) be given by

$$H_{r,c} = \left. \frac{\delta f_r}{\delta x_c} \right|_{\mathbf{x}} \quad (16)$$

Then, assuming  $X$  input features we can use the existing  $N \times X$  Jacobian, to calculate the new  $N \times m$  Jacobian in terms of  $\mathbf{x}'$  rather than  $\mathbf{x}$ , using the chain rule:

$$\begin{aligned} H'_{r,c} &= \frac{\delta f_r(\mathbf{x})}{\delta x'_c} \\ &= \frac{\delta f_r(\mathbf{x})}{\delta x_1} \cdot \frac{dx_1}{dx'_c} + \dots + \frac{\delta f_r(\mathbf{x})}{\delta x_n} \cdot \frac{dx_n}{dx'_c} \\ &= H_{r,1} p_{c,1} + \dots + H_{r,n} p_{c,n} \\ &= \nabla_{\mathbf{x}} f_r(\mathbf{x}) \cdot \mathbf{p}_c \end{aligned} \quad (17)$$

where  $\mathbf{p}_c$  is the  $c^{\text{th}}$  row of  $P$ , transposed. Then each row  $\mathbf{h}'_r$  of the new Jacobian in terms of  $\mathbf{x}'$  is given by

$$\mathbf{h}'_r = \nabla_{\mathbf{x}} f_r(\mathbf{x}) P^T \quad (18)$$

Equation (18) which can be used directly in the adjusted version of Equations (11) and (12), such that

$$\begin{aligned} \mathbf{d} &= \frac{f_i(\mathbf{x}) - f_j(\mathbf{x})}{\|\mathbf{h}'_j - \mathbf{h}'_i\|_2} (\mathbf{h}'_j - \mathbf{h}'_i) \\ &= \frac{f_i(\mathbf{x}) - f_j(\mathbf{x})}{\|(\nabla_{\mathbf{x}} f_j(\mathbf{x}) - \nabla_{\mathbf{x}} f_i(\mathbf{x})) P^T\|_2} (\nabla_{\mathbf{x}} f_j(\mathbf{x}) - \nabla_{\mathbf{x}} f_i(\mathbf{x})) P^T \end{aligned} \quad (19)$$

$$\text{and } \|\mathbf{d}\|_2 = \frac{f_i(\mathbf{x}) - f_j(\mathbf{x})}{\|[\nabla_{\mathbf{x}} f_j(\mathbf{x}) - \nabla_{\mathbf{x}} f_i(\mathbf{x})] P^T\|_2} \quad (20)$$

In effect, we start at point  $\mathbf{x}$  (the only point we have a model output for), and then use the gradient in the lower dimensional space to find the minimal distance  $\|\mathbf{d}\|_2$ .